

多功能秸秆纤维基可视化智能标签的构筑和性能表征

刘若婷¹ 宁语革¹ 任子豪¹ 许士玉¹ 程倩¹ 杨冬梅¹ 王立娟^{1*}

(1. 东北林业大学 哈尔滨 150000)

摘要: 智能标签可以实时提供食品新鲜度信息。然而, 现有研究的智能标签 pH 响应范围窄, 只能监控单一食品的质量, 阻碍了其实际应用。为了突破这个瓶颈问题, 本研究设计了一种响应范围宽、指示精度高、高效抑菌的纤维素基智能标签用于监控猪肉、牛奶、菠菜的新鲜度。利用草酸改性秸秆纤维素纤维引入羧基基团 (-COO⁻), 通过静电作用键合带正电荷的壳聚糖季胺盐, 进一步吸附阴离子复合染料-甲基红和溴百里香酚蓝, 最后自组装成智能标签。壳聚糖季胺盐的引入有效地改善了标签的拉伸强度和断裂伸长率, 两者分别增加了 282% 和 16.2%; 同时赋予了其优良的抑菌性能, 对金黄色葡萄球菌的抑菌率高达 100%。在 pH 范围为 3-9 时, 该标签呈现了截然不同的高饱和度颜色; 遇乙酸蒸汽由绿色转变为粉色, 遇氨气又迅速地变回绿色, 表明了该智能标签具有快速的酸-碱气体响应性及可逆性。将标签应用于监测猪肉、牛奶以及菠菜的新鲜度, 标签从绿色逐渐转变为橘黄色, 表明牛奶/菠菜质量状态由新鲜转变为濒临腐败; 由绿色转变为黄色, 再继续变为浅绿色表明了猪肉质量状态由新鲜到可接受再到濒临腐败的过程。本研究提供了一种可有效地将废弃稻草秸秆纤维高值化转变为多应用范围智能标签的途径, 符合节约型社会及国家经济可持续发展理念。

关键词: 智能纤维素纤维标签; 复合染料; 高辨识度; 宽响应范围; 食品新鲜度

An antibacterial and intelligent cellulose-based label self-assembled via electrovalent bonds for a multi-range sensing of food freshness

Abstract: Intelligent labels provide customers with food freshness information. However, the existing label response is limited and can only detect a single kind of food. Here, an intelligent cellulose-based label with highly antibacterial activity for a multi-range sensing freshness was developed to overcome the limitation. Cellulose fibers were modified using oxalic acid to graft -COO⁻ followed by binding chitosan quaternary ammonium salt (CQAS), the remaining charges of which attached methylene red and bromothymol blue to form response fibers and to further self-assemble into the intelligent label. CQAS electrostatically gathered the dispersed fibers, resulting in an increase in TS and EB of 282% and 16.2%, respectively. After that, the rest positive charges fixed the anionic dyes to broaden pH response range of 3-9 effectively. More significantly, the intelligent label exhibited highly antimicrobial activity, killing 100% of staphylococcus aureus. The rapid acid-base response revealed the potential for practical application in which the label color from green to orange represented the milk or spinach from fresh to close to spoiled, and from green to yellow, and to light green indicated the pork fresh, acceptable, and close to spoiled. This study paves a way for the preparation of intelligent labels in large-scale and promote the commercial application to improve food safety.

Key words: Intelligent cellulose-based label; Multi-range sensing; Food freshness.

1 Introduction

Proteins and vitamins are important in the activities throughout living cells and organisms (Cao et al., 2019), with which has spurred the consumption of diets supplemented (Milisav et al., 2018). The protein-rich foods include meat, milk, soybeans, eggs, fish, and shrimp. Vegetables enriched in carotenoids, vitamin C, vitamin K, minerals, calcium, iron, and other nutrients are spinach, broccoli, celery, and cabbage. However, these foods are prone to spoil

基金项目: 黑龙江省自然科学基金重点项目 (ZD2020C003)

* 王立娟为通讯作者

due to microorganism activity during transportation and storage. Eating low-quality food could be a health risk for humans (Chi et al., 2020; Yang et al., 2021). Therefore, the identification of food freshness is urgent and important. Traditional physicochemical analyses and microbial growth assays are not consumer oriented, as they require a variety of chemical reagents, personnel with expertise, and time, which are difficult for consumers to conduct (Gökodlu et al., 2008; Kuswandi and Nurfawaidi, 2017). Intelligent indicators responding to temperature (Brizio and Prentice, 2015), humidity (Rahman and Chowdhury, 2022), organic gases (Zhang et al., 2022), and pH (Ezati et al., 2023) in the form of color shifts have received increasing attentions due to its accuracy, rapidity, and easy operation (Sun et al., 2019).

Generally, the activity of microorganisms in food often leads to pH changes in the environment surrounding the food, due to the generation of organic acids, total volatile basic nitrogen (TVB-N), and CO₂. Thus, evaluating food freshness by monitoring pH changes is convenient (Liu et al., 2019). Recently, pH-sensitive indicators have been developed by mixing synthetic dyes into the polymer matrix (Teixeira et al., 2022). Bromocresol green with a pH response range of 3.6–5.2 had been encapsulated into cellulose acetate to monitor the freshness of fish (Pacquit et al., 2006). Bromocresol purple that shifting color over a pH range of 5.2–6.8 was immobilized on the filter paper for monitoring chicken breast freshness (Kim et al., 2017). Bromothymol blue (BTB) with a color change at pHs ranging from 6.0–7.6 was fixed to sodium carboxymethyl cellulose and carrageenan to monitor the quality of fresh-cut papaya (Rong et al., 2023). These innovations have promoted the development of pH-sensitive films. However, each of these films containing a single dye could monitor only acidic or alkaline changes due to the narrow pH range, which has limited the further development of the pH-sensitive film for practical applications.

Currently, mixed indicators with more accurate test results consisting of two or more types of dyes have been developed to break down the limitation, which can make it easy to detect the threshold of spoilage and different freshness levels of food, avoiding false positives and negatives (Ran et al., 2021). Chen et al. embedded BTB and methylene red (MR) in a polymer matrix to form a composite indicator with a pH response ranging from 4.4–7.1. This system was used for monitoring the freshness of pork based on the TVB-N level and fresh-cut green pepper based on the CO₂ level (Chen et al., 2019; Chen et al., 2018). The mixed indicator effectively expanded the pH-response range comparing with the single one, improving the indication accuracy and achieving the freshness monitoring for multiple foods.

Unfortunately, while achieving accurate indication, safety cannot be ignored. Simple blend may cause the migration of toxic dyes into foods (Cao et al., 2019). Incalculable harm to human health following ingestion of synthetic dyes is at least theoretically possible. Thus, firm anchoring of the dyes on the test surface is necessary to ensure food safety. In our previous work, BTB was adsorbed on quaternized cellulose fibers to indicate the freshness of fish and pork via ionic bonds (Liu et al., 2022). However, quaternization of cellulose fibers requires toxic chemical reagents and a more complicated synthesis process. Hence, a simple, efficient, and eco-friendly method for dye immobilization is urgently needed. The polyelectrolyte complexes formed via two biopolymers carrying opposite charges are regarded as the suitable candidate to anchor dyes firmly. Here, it was constructed by binding long-chain chitosan quaternary ammonium salt with high-density of positive charges to the carboxylated cellulose fibers, which could be achieved using oxalic acid (OA) (Jiang et al., 2021), acetic acid (Wang, H. et al., 2020), and

maleic acid (Bian et al., 2019). Among them, OA was selected as an esterifying agent due to its natural-richness, sustainability, biocompatibility, and biodegradability (Palmieri et al., 2019). It is supposed that the prepared polyelectrolyte complexes can achieve the adsorption for anionic dyes, and then, conduct the multi-range monitoring of food freshness.

Herein, with the goals of carbon neutrality and green chemistry, we report an efficient method utilizing cellulose fibers to prepare a multi-range pH sensing label for monitoring food freshness. The -COOHs from OA were introduced onto cellulose fibers to bind partial positive charges of CQAS, the residue positive charges of which were used to attach BTB and MR to obtain response fibers. They self-assembled to form the intelligent label. The surface morphologies, element composition, functional groups, and thermal stability were characterized using Scanning electron microscope (SEM), X-ray photoelectron spectrometry (XPS), Energy dispersive spectroscopy (EDS), Fourier transform infrared spectrometry (FTIR), X-ray diffraction (XRD), and thermogravimetric analysis (TGA). For the label, the hygroscopicity, mechanical property, antibacterial activity, pH sensitivity, and acid-base gases response property were tested. In addition, the practical applications of the label in milk, pork, and spinach freshness monitoring were investigated.

2. Experimental section

2.1 Materials

Cellulose was from rice straw pulp. Oxalic acid ($\text{H}_2\text{C}_2\text{O}_4$), bromothymol blue ($\text{C}_{27}\text{H}_{28}\text{O}_5\text{SBr}_2$) and methyl red ($\text{C}_{15}\text{H}_{15}\text{N}_3\text{O}_2$) were provided by Kemiou Chemical Reagent Co., Ltd (Tianjin, China). Chitosan quaternary ammonium salt (CQAS) was purchased from Lushen Bioengineering Co., Ltd. (Jiangsu, China).

2.2 Synthesis of the cellulose-based polyelectrolyte complexes

Firstly, 2 g of pristine cellulose fibers (CF) was dispersed into 100 mL oxalic acid/water solution with different concentrations (10%, 15%, 20%, 25%, 30%, 40% and 50%), and the mixture was stirred with a speed range of 0-2600 r/min (stepless speed regulation) continuously at 80 °C for 1 h. After the reaction, ethanol was added into above solution to dissolve excess oxalic acid, and then that was retrieved by the rotary evaporation. The obtained product was washed using ethanol until the conductivity of filtrate didn't change. The carboxyl content of the OA-treated cellulose fibers (OACF) was measured via the method in the reference (Rohaizu and Wanrosli, 2017). Subsequently, 2 g of OACF was mixed with 100 mL CQAS aqueous solution (5 g/L, 10 g/L, 15 g/L, 20 g/L, 25 g/L and 30 g/L) with a stirring range of 0-2600 r/min (stepless speed regulation) at 25 °C for 2 h. After that, the product was filtrated and washed with distilled water, dried at 60 °C for 12 h, and named as CQ-OACF.

2.3 Preparation of the cellulose-based label

The composite dyes solvent was obtained via mixing bromothymol blue and methyl red with a ratio of 1:1 (w/w) into NaOH solution (0.05 mol/L). CQ-OACF was immersed into dyes solution with a shaking speed of 150 rpm under 30 °C until the adsorption reached an equilibrium. After filtering, the precipitate was firstly washed with 0.05 mol/L NaOH solution to remove the physically attached dyes, and then with a lot of deionized water until the pH of filtrate was 7. The cellulose-based label was prepared by the vacuum-assisted filtration, and dried overnight at 60 °C for further use. In addition, the pristine cellulose fibers, carboxylated cellulose fibers and polyelectrolyte complexes were self-assembled to construct the three-dimensional matrix, named PF matrix, CF matrix, and PC

matrix as controls, respectively.

2.4 Characterizations

The changes of pristine cellulose during the modification were observed by an iPhone 13, and the microscopic morphology and surface elements were researched using Scanning electron microscope (SEM, Apreo S HiVac, Thermo Scientific, MA, America) and Energy dispersive spectrometer (EDS). The researches of functional groups were conducted using Fourier transform infrared spectra (FTIR) in the range of 4000~500 cm^{-1} (Nicolet iS50, Thermo fisher, Shanghai, China) and X-ray photoelectron spectroscopy (XPS, AXIS Ultra DLD, Kratos, Manchester, UK). The crystal structures were studied via X-ray diffraction (XRD, D/max 2200, Rigaku Corporation, Tokyo, Japan). Thermogravimetric analysis (TGA) was conducted using a TA instruments (TGA Q500, TA Instruments, USA) from 25 to 600 °C at a heating rate of 10 °/min to assess the thermal properties of samples. The contact angle was measured with 5 μL of water droplets using a DSA25 instrument (KRUSS, Hamburg, Germany).

2.5 Moisture adsorption test

The PF matrix, CF matrix, PC matrix, and intelligent label were cut into 6 mm×6 mm and placed in various relative humidity conditions (11%, 22%, 33%, 43%, 53% and 75%), and then, the weight of each was measured within a certain time interval until it didn't change. The moisture rate (M%) was calculated by the following formula:

$$M\% = (m_2 - m_1) / m_1 \times 100\%$$

where m_1 and m_2 are the weights of the samples at the beginning and time t, respectively.

2.6 Mechanical properties

The PF matrix, CF matrix, PC matrix, and intelligent label were cut into 15.0 mm × 80.0 mm and placed in various RH conditions (11%, 22%, 33%, 43%, 53% and 75%) until that reached a moisture equilibrium. Mechanical properties containing tensile strength (TS) and elongation at break (EB) were evaluated with an auto tensile tester (XLW-PC; Labthink; China) with a stretch rate of 300 mm/min.

2.7 Release test

The release behavior of the intelligent label was assessed in 50% and 95% ethanol aqueous (as food stimulants). 0.1 g of the label was immersed into 50 mL food stimulants and shook for 24 h under a speed of 200 rpm. Then, the absorbance of solution was measured using UV-spectrophotometer. The 50% and 95% ethanol aqueous were used as controls.

2.8 Antimicrobial activity

A shake-flask method was used to evaluate the antimicrobial activity. 0.2 g of samples was cut into small pieces, and immersed into bacteria suspension (1 mL) and PBS buffer (9 mL), oscillating under a speed of 180 rpm/min for 1 h at 37 °C. Then, taken out 0.2 mL of suspension and coated it on a nutrient agar plate, culturing at 37 °C for 12 h. The antimicrobial rate (R) was got via the following formula:

$$R = (A_1 - A_2) / A_1 \times 100\%$$

where A_1 and A_2 are the colonies number of the control group and tested samples, respectively.

2.9 pH response

The label was cut into a circular with a diameter of 1 cm and immersed into different pH buffer solutions for 30 s. Then, the image was recorded by an iPhone 13, and the chromaticity parameters (L, A, B) were measured using

a handheld colorimeter. ΔE was got using the following formula:

$$\Delta E = [(L-L_i)^2 + (A-A_i)^2 + (B-B_i)^2]^{1/2}$$

where L_i , A_i and B_i are the chromaticity parameters of initial cellulose-based label, that are denoted by L , A , and B after response, respectively.

2.10 Acid-base gas response

The labels (0.6 cm×0.6 cm) were placed in plastic containers (450 mL) with different humidity environment (33%, 53%, 75%) for 48 h. Then, 5 mL acetic acid or triethylamine solution was injected with a syringe to observe the color changes of label at a fixed time interval (30 s, 60 s, 300 s, 600 s, 900 s, 1200 s).

2.11 Tracking the freshness of three foods

For pork, each group (90 g) with coverage of the cellulose-based label (0.6 cm×0.6 cm) was sealed in a sterilized petri dish, and then placed at 20 °C. For the evaluation of pork freshness during the storage, the TVB-N level was tested using the method in the reference (Chi et al., 2020).

Fresh spinach was soaked in sodium hypochlorite solution (v/v, 100 μL/L) for 10 min, and rinsed with a lot of water, then, placed in a self-sealed bag with the labels inside. Weight loss of spinach was assessed at intervals, meanwhile the chlorophyll content was tested according to the method (Chen et al., 2018). The aerobic plate counts were applied to evaluate the number of microorganism (CFU; \log_{10} CFU g⁻¹) referring to the Chinese standard GB 4789.2-2022.

2.12 Statistical analysis

Three replicates of each experiment were conducted, and all data was studied by SPSS (v17.0, Chicago, USA). The final result was showed as mean±standard deviation with a significant difference of $P < 0.05$.

3. Results and discussion

3.1 Preparation and characterizations of the cellulose-based polyelectrolyte complexes

The preparation diagram is shown in Figure 1. The zeta potential of the CF was -4.71 mV. That of OACF decreased to -22.50 mV after the OA treatment (Table 1), proving the successful introduction of carboxyl groups (Li et al., 2017). After bonding CQAS, the zeta potential increased to +48.6 mV, which is beneficial for adsorbing anionic dyes.

Tab. 1 Zeta potential of CF, OACF, and CQ-OACF.

Sample	Zeta potential (mV)
CF	-4.71
OACF	-22.50
CQ-OACF	48.60

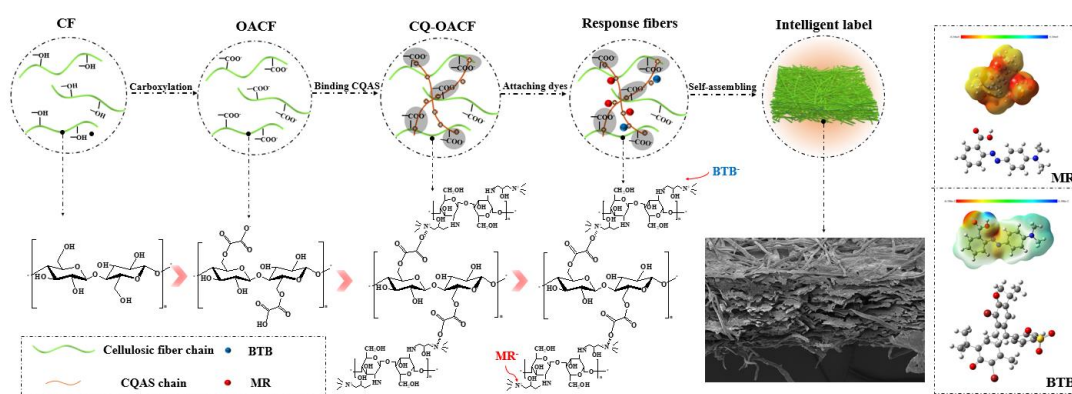


Fig. 1 Mechanism diagram of the process to prepare the intelligent cellulose-based label

Figure 2 shows SEM images of CF, OACF, and CQ-OACF. The surface of CF was wrinkled because the removal of lignin made the cell wall collapse (Figure 2d-j) (Liu et al., 2022). After carboxylation, the length of fibers decreased because OA removed the amorphous and less ordered regions in them (Moon et al., 2011) (Figure 2e). For CQ-OACF, a thin CQAS film occurred on the surface of OACF (Figure 2f-2i). Moreover, it can be seen that CQAS effectively connected the dispersed fibers to form a cross-linked structure (Figure 2f).

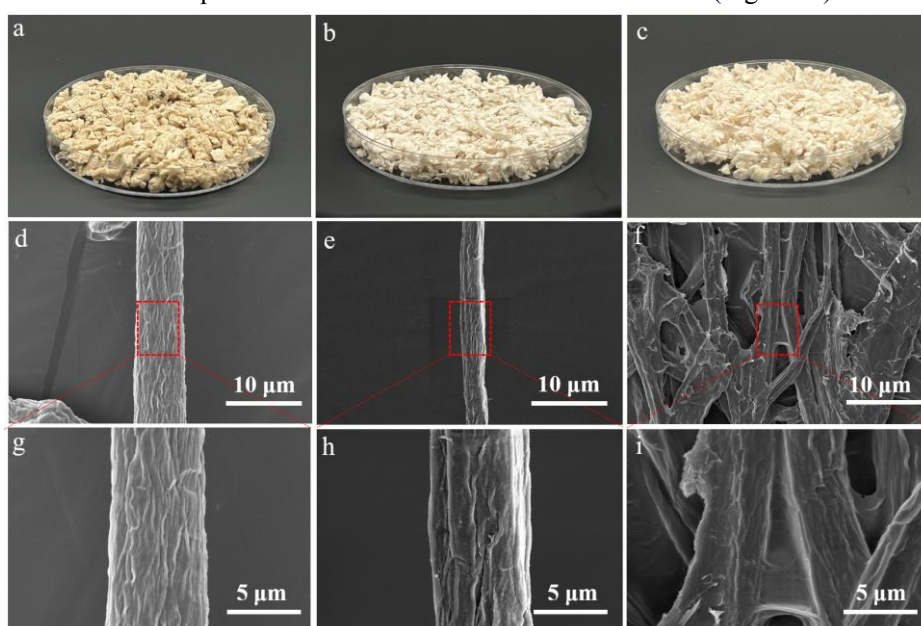


Fig. 2 Photos and SEM images of CF (a, d, g), OACF (b, e, h), and CQ-OACF (c, f, i)

The reaction mechanism was assessed using XPS and FTIR analyses. Figure 3a–f present the high-resolution spectra of C1s and N1s in CF, OACF, and CQ-OACF. For CF, the XPS spectrum of C1s was curved-fitted into three peaks with a binding energy of 283.25 eV for C–C, 284.91 eV for C–O, and 285.98 eV for O–C–O (Li et al., 2020). The XPS spectrum of N1s exhibited a peak at 398.38 eV, which may be due to the nitrogen compounds of rice straw cellulose [20]. After carboxylation, the new C1s peak at 286.70 eV contributed to the introduced –COOH, which was beneficial for bonding CQAS. The N1s peak at 398.38 eV implied the carboxylation had no significant effect on the nitrogen compounds. For the N1s spectrum of CQ-OACF (Figure 3f), three fitting peaks were centered at 401.21 eV, 398.61 eV, and 397.75 eV attributing to N⁺ in CQAS, N1s in the nitrogen compounds of rice straw cellulose, and N–H in CQAS, respectively.

FTIR was used to further disclose the changes of functional groups during modification. In the spectrum of CF (Figure 3g), the peaks at $3200\text{--}3650\text{ cm}^{-1}$ and 1639 cm^{-1} represented the stretching vibration and bending vibration of --OH . The peaks at 1056 and 897 cm^{-1} were assigned to the stretching vibration of C--O and C--O--C , which are the characteristic absorption bands of cellulose and hemicellulose, respectively (Jiang et al., 2022). For OACF, the new peak appeared at 1730 cm^{-1} representing the stretching vibration of C=O (Figure 3h), which further proved the successful carboxylation of CF (Jiang et al., 2021) (Li et al., 2017). As seen in Figure 3i, the FTIR spectrum of CQ-OACF included a peak at 1480 cm^{-1} , which was from the quaternary ammonium salt side chain (Chi et al., 2023).

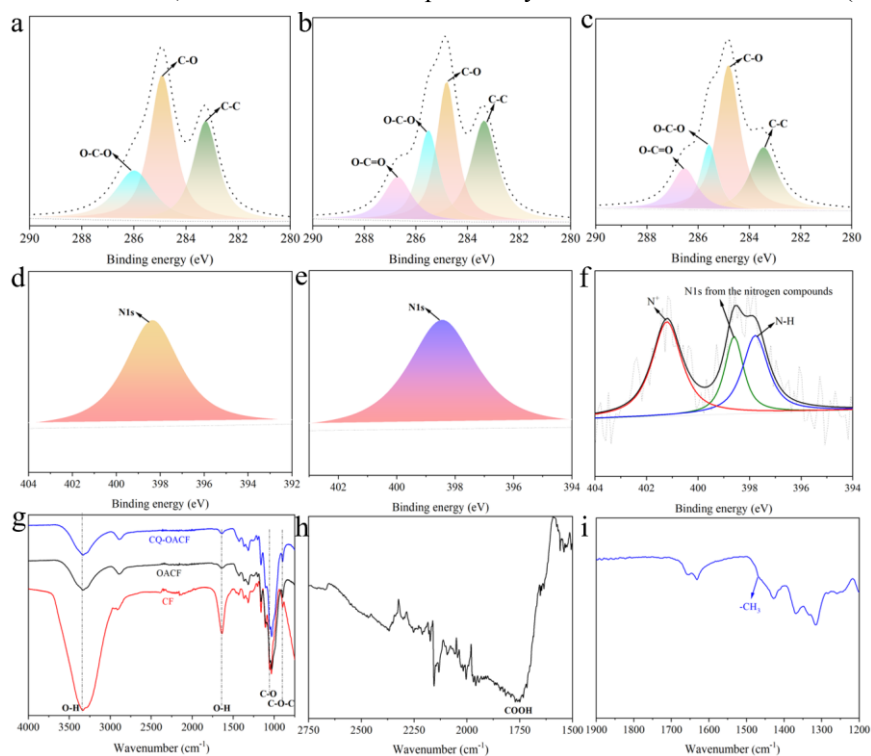


Fig. 3 High resolution XPS spectra of C1s and N1s: CF (a–d), OACF (b–e), and CQ–OACF (c–f); FTIR spectra of CF, OACF, and CQ–OACF (g–i); EDS spectra of CF (g), OACF (k), and CQ–OACF (l), respectively

3.2 Dyes attaching of CQ-OACF and self-assembly of response fibers

The polyelectrolyte complexes (CQ-OACF) with more positive charges were used to attach MR and BTB carrying negative charges in alkali solution to prepare the response fibers. Figure 4a shows that the adsorption capacity for BTB increased from 13.71 to $21.33\text{ }\mu\text{mol/g}$ and for MR from 16.76 to $25.51\text{ }\mu\text{mol/g}$ with OA concentration increasing from 10% to 50% , respectively. Higher OA concentration could introduce more negative charges on the CF, binding more CQAS and attaching increased dyes. As shown in Figure 4b, the adsorption capacity for BTB increased slowly from 19.02 to $21.36\text{ }\mu\text{mol/g}$ and for MR from 22.52 to $24.47\text{ }\mu\text{mol/g}$ as the CQAS concentration increased from 0.5% to 3% , and that reached a saturation at CQAS concentration $\geq 2\%$. Besides, the adsorption capacity for MR was always higher than that for BTB because of the lower molecular weight and the smaller steric hindrance of MR comparing with BTB, thus MR could occupy the adsorption site rapidly to achieve higher adsorption capacity. Simultaneously, the pristine cellulose fibers were directly used to adsorb dyes as controls. Figure 4c revealed that the dyes adhered to the pristine cellulose fibers were easily washed away by alkali, proving that there was no chemical bonding between them. Figure 4d shows the migration rates of BTB and MR from CQ-

OACF in the 50% and 95% ethanol aqueous solutions were close to zero, further confirming the effective binding of MR and BTB to the cellulose-based polyelectrolyte complexes.

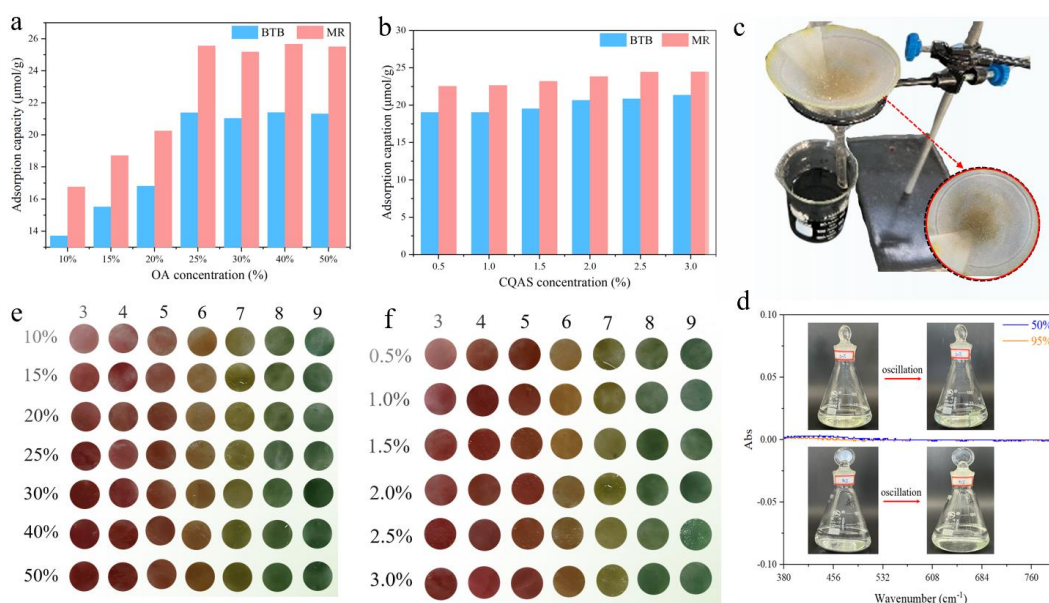


Fig. 4 Adsorption capacity prepared under different conditions: OA concentration (a); CQAS concentration (b); dyes adsorption by pristine cellulose (c); dye migration in 50% and 95% ethanol solution (d); pH response of intelligent label prepared under different conditions: OA concentration (e); CQAS concentration (f); gas response device (g); acetic acid response (h); triethylamine response (i)

The intelligent labels were obtained by the self-assembly of response fibers (Figure 5a). SEM was applied to inspect the microstructure. The response fibers intertwined to construct the label matrix via hydrogen bonds (Figure 5b) (Shi and Wu, 2021). Although there was a thin CQAS layer on the fibers surface (Figure 5c), many holes could still be observed, causing the rapid penetration of water droplets assisted with the capillarity once liquid contacted the label surface. This structure could achieve the quick detecting of milk and the diffusion of the tested gas.

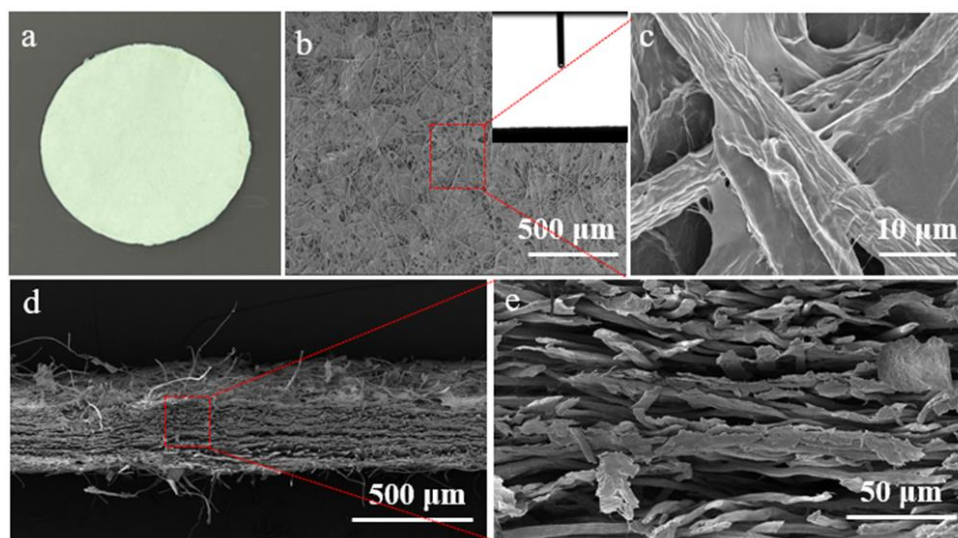


Fig. 5 Photos (a) and SEM images (b, c, d, e) of intelligent label

3.3 Dimensional stability and security

3.3.1 Hygroscopic capacity

The hygroscopic capacity of the PF matrix, CF matrix, PC matrix, and intelligent label was evaluated by placing them in various RHs (11%, 22%, 33%, 43%, 53%, and 75%). During the storage, the cellulose-based samples gradually adsorbed moisture from the surrounding environment until an equilibrium. All the matrices consistently adsorbed moisture because that the hydrophilic groups (-OH, -COOH, -NH) can form hydrogen bonds with the water molecules. However, the hygroscopic capacity is different for different cellulose-based matrices. The equilibrium moisture adsorption rates at 75% RH in Figure 6(a-d) are reported as follows: PF matrix of 4.71%, CF matrix of 5.46%, PC matrix of 8.64%, and the intelligent label of 3.58%, indicating that the CF matrix could provide more hydrophilic sites, such as -OH and -COOH, and CQAS further improved the moisture adsorption/retention properties of the cellulose-based matrix. It is worth noted that the intelligent label showed a weaker hygroscopic capacity than PF matrix, CF matrix, and PC matrix because that the intelligent label containing more hydrophobic components (MR and BTB) and less hydrophilic groups. The weaker hygroscopic capacity endowed the intelligent label with a better dimensional stability, avoiding the inconspicuous discoloration for swelling, and deformation due to moisture absorption in practical applications.

3.3.2 Mechanical properties

The mechanical properties of PF matrix, CF matrix, PC matrix, and intelligent label are shown in Figure 6e-f, and the sort of that was PC matrix > PF matrix > intelligent label > CF matrix, revealing the modification had an interesting effect on those. Initial cellulose fibers matrix (PF matrix) exhibited TS and EB of 11.18 MPa and 3.7%, respectively. After carboxylation, the length of cellulose fibers greatly decreased, which led to not only less interfibrous bonding, but also a low retention rate, causing the poor mechanical properties (TS of 3.03 MPa and EB of 3.1%) (Hu et al., 2021). These were improved by the binding of CQAS, increasing TS and EB to 11.58 MPa and 3.7% because CQAS could electrostatically gather shorter fibers to prevent them losing, similar result has been previously reported (Fernandes et al., 2009). As seen in Figure 6(e-f), TS and EB of the intelligent label decreased to 9.28 MPa and 3.18% because the adsorption of dyes competed the positive charges of CQAS to reduce the interaction with the OACF. As shown that humidity has a slight effect on the mechanical properties of the intelligent label. TS of that decreased from 10.58 to 9.17 MPa and EB increased from 2.37% to 3.24% as RH increased from 11% and 75%. More moisture could decrease the stiffness of the fibers and destroy the hydrogen bonds between fibers, thus resulting in the decrease of tensile strength (Meng and Wang, 2019; Spiewak et al., 2022).

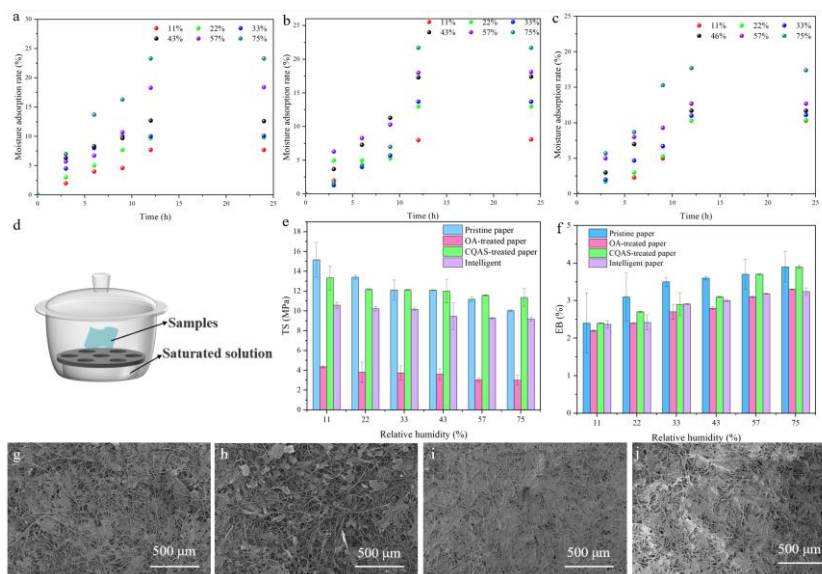


Fig. 6 Moisture adsorption properties of PF matrix (a), PC matrix (b) and intelligent paper (c); the constant humidity device (d); EB (e) and TS (f) of samples; SEM images of PF matrix (g), CF matrix (h); PC matrix (i) and intelligent label (j)

3.4 Antibacterial activity

As is known that CQAS has a superior antibacterial activity against most gram-negative and gram-positive bacteria (Wang, A. et al., 2020). Thus, we hypothesized that the intelligent label containing CQAS would exhibit a similar activity. The results in Figure 7a, b, e, f showed that PF matrix and CF matrix exhibited poor antibacterial activity against *E. coli* and *S. aureus*. However, PC matrix and the intelligent label demonstrated remarkable antibacterial activity against *E. coli* (98.3%, 91.7%) and *S. aureus* (100%, 100%), which may be due to that the positive charges of CQAS could destroy the negatively charged bacteria membranes (Yu et al., 2022). In addition, it is found that the inhibition rates of all samples against *S. aureus* were higher than that against *E. coli* due to the external lipidic membrane in gram-negative. The excellent antibacterial properties could negate the interference from bacteria to the color change for the intelligent label which would objectively and correctly reflect food freshness.

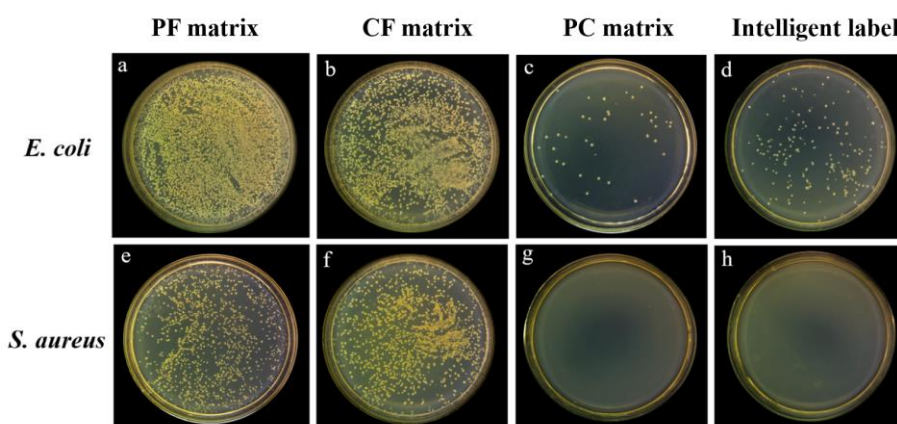


Fig. 7 Antibacterial properties of PF matrix (a-e), CF matrix (b-f), PC matrix (c-g), and intelligent paper (d-h) against *E. coli* and *S. aureus*

3.5 pH Response

pH sensitivity is critical for tracking food quality. Thus, we measured the response to solutions with pHs ranging from 3 to 9 using the intelligent label. As seen in Figure 4e–f, the intelligent label colors showed pink at pH 3–4, saffron yellow at pH 5, yellow at pH 6, green at pH 7, light green at pH 8; and blue–green at pH 9. The color parameters (L^* , a^* , and b^*) of the intelligent label were also recorded. The a^* value decreased with an increased pH, indicating a color shifted from red to green. The b^* value initially increased and then decreased, and reached a maximum value at pH 6, indicating a shift to yellow at pH < 6 and a shift to blue at higher pH values (shown in Figure S6). The obtained ΔE exceeded 5, indicating that the color changes would be easily recognized by experienced and inexperienced observers (Jamroz et al., 2019).

3.6 Monitoring tests

During the storage of pork, carbohydrates are decomposed to produce organic acids and CO_2 , and proteins are decomposed to produce basic nitrogen compounds (TVB–N) due to enzyme activity and decomposition of bacteria. In this study, TVB–N was the preferred choice because it increased along with the spoilage of pork, and that of acceptable pork is 15 mg/100 g according to the Chinese National Standard GB2707–2016. As shown in Figure 8, the initial TVB–N value of fresh pork was 6.19 mg/100 g, and the cellulose-based label was green. Over time, the value of TVB–N rapidly increased due to the protein decomposition, and reached 14.86 mg/100 g after 24 h, which is close to the threshold (15 mg/100g). In this process, the label exhibited light green, yellow, and green after 14, 19, and 24 h, respectively. These changes occurred because the glycogen of meat was firstly decomposed by rotting bacteria to produce lactic acid and CO_2 , thus the label changed from green to light green, and to yellow at this stage. After the glycogen was exhausted, protein would begin to decompose (Lin et al., 2022). The headspace environment would gradually change to alkaline, with a corresponding change in color of the label from yellow to green, providing a warning of pork freshness.

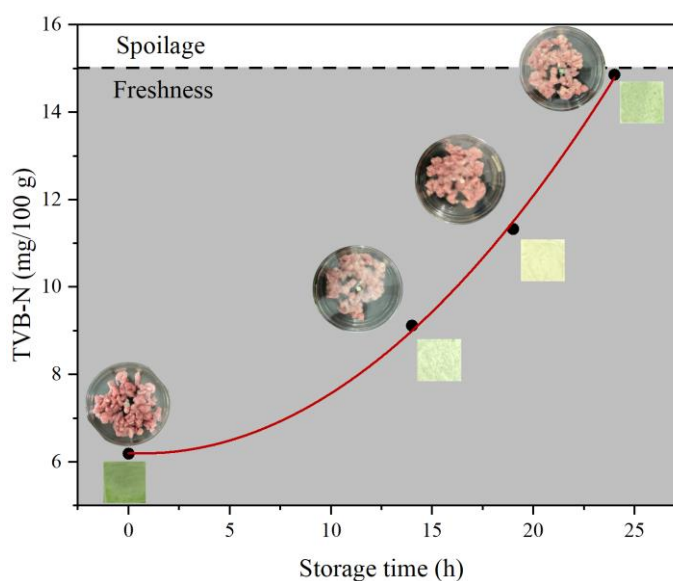







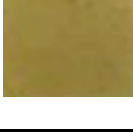


Fig. 8 TVB–N changes of pork with the storage time

Fresh spinach is very popular due to its enriched contents of folic acid, vitamin C, vitamin K, carotenoid, calcium, iron, and other nutrients. However, spinach is an ideal medium for the growth of various microorganisms, which could compromise the safety of the vegetable. Thus, a label that can reflect the aerobic plate count will be valuable.

Table 2 summarizes the changes of characteristic indicators of spinach during refrigerated storage. The chlorophyll content and aerobic plate count of fresh spinach were 1.42% and 1.6 log₁₀ CFU g⁻¹, respectively, indicating the excellent state of the spinach. As the storage time increased, the mass loss increased to 5.17% due to transpiration, and the chlorophyll content slightly decreased to 1.21%, reflecting the degradation caused by oxygen and enzymes. The aerobic plate count increased to 4.5 log₁₀ CFU g⁻¹. Other studies have established that an aerobic plate count of 5.0 log₁₀CFU g⁻¹ is the preferred threshold of edible fresh vegetables. Thus, spinach could be divided into four states during storage: very fresh, fresh, acceptable, and close to the tolerance limit. Accordingly, the intelligent label in each stage was colored green, yellow–green, yellow, and orange, respectively, which were readily discernable to the naked eye.

Tab. 2 Changes of characteristic indicators of spinach during refrigerated storage.

Stored time (d)	Mass loss (%)	Chlorophyll content (%)	Aerobic plate count (log ₁₀ CFUg ⁻¹)	Status	discoloration
0	0	1.42±0.05 ^c	1.6±0.1 ^b		
3	1.97±0.01 ^a	1.33±0.02 ^a	3.9±0.2 ^a		
6	3.35±0.03 ^a	1.27±0.02 ^a	4.2±0.5 ^a		
9	5.17±0.01 ^c	1.21±0.01 ^c	4.5±0.7 ^a		

4. Conclusions

A safe intelligent cellulose–based label with a multi–range pH sensing was fabricated. CQAS with high density positive charges was bound onto carboxylated cellulose to anchor BTB and MR for monitoring of food freshness. OA was used to provide –COOH for cellulose. A higher concentration of OA (≥25%) could improve thermal stability and crystallinity. The bound CQAS could electrostatically link BTB and MR, effectively extending the pH response range from 3 to 9, and endowing the cellulose–based label with excellent antibacterial ability (100% killing) against *S. aureus*. More importantly, the intelligent label showed a remarkable performance response for pH, acetic acid, and triethylamine. Monitoring testing demonstrated a real–time, visual, and safe detection of the freshness of milk, pork and spinach. The collective results demonstrate the promising potential of the intelligent label to track the freshness of a wide range of foods.

References

- Bian H Y, Luo J, Wang R B, *et al.* 2019. Recyclable and Reusable Maleic Acid for Efficient Production of Cellulose Nanofibrils with Stable Performance. *Acs Sustainable Chemistry & Engineering*, 7(24):20022-20031.
- Brizio A P, Prentice C. 2015. Development of an intelligent enzyme indicator for dynamic monitoring of the shelf-life of food products. *Innovative Food Science & Emerging Technologies*, 30:208-217.
- Cao L, Ma Q, Liang T, *et al.* 2019. A semen cassia gum-based film with visual-olfactory function for indicating the freshness change of animal protein-rich food. *International journal of biological macromolecules*, 133:243-252.
- Chen H z, Zhang M, Bhandari B, *et al.* 2019. Development of a novel colorimetric food package label for monitoring lean pork freshness. *Lwt*, 99:43-49.
- Chen H Z, Zhang M, Bhandari B, *et al.* 2013. Applicability of a colorimetric indicator label for monitoring freshness of fresh-cut green bell pepper. *Postharvest Biology and Technology*, 140:85-92.
- Chi W, Cao L, Sun G, *et al.* 2020. Developing a highly pH-sensitive κ -carrageenan-based intelligent film incorporating grape skin powder via a cleaner process. *Journal of Cleaner Production*, 244:118862.
- Chi W, Liu W, Xu S, *et al.* 2023. A new strategy to glue-seal κ -carrageenan film for packaging grease. *Journal of Food Engineering*, 337:111248.
- Ezati P, Khan A, Rhim J W, *et al.* 2023. pH-Responsive strips integrated with resazurin and carbon dots for monitoring shrimp freshness. *Colloids and surfaces. B, Biointerfaces*, 221:113013.
- Fernandes S C M, Freire C S R, Silvestre A J D, *et al.* 2009. A study of the distribution of chitosan onto and within a paper sheet using a fluorescent chitosan derivative. *Carbohydrate polymers*, 78(4):760-766.
- Gökodlu N, Özden Ö, Erkan N. 2008. Physical, Chemical and Sensory Analyses of Freshly Harvested Sardines(*Sardina pilchardus*) Stored at 4°C. *Journal of Aquatic Food Product Technology*, 7(2):5-15.
- Hu F, Zeng J, Cheng Z, *et al.* 2021. Cellulose nanofibrils (CNFs) produced by different mechanical methods to improve mechanical properties of recycled paper. *Carbohydrate polymers*, 254:117474.
- Jamroz E, Kulawik P, Krzysciak P, *et al.* 2019. Intelligent and active furcellaran-gelatin films containing green or pu-erh tea extracts: Characterization, antioxidant and antimicrobial potential. *International journal of biological macromolecules*, 122:745-757.
- Jiang J, Chen X, Zhang G L, *et al.* 2022. Preparation of chitosan-cellulose-benzyl isothiocyanate nanocomposite film for food packaging applications. *Carbohydrate polymers*, 285:119234.
- Jiang J, Zhu Y, Zargar S *et al.* 2021. Rapid, high-yield production of lignin-containing cellulose nanocrystals using recyclable oxalic acid dihydrate. *Industrial Crops and Products*, 173:114148.
- Kim D, Lee S, Lee K, *et al.* 2017. Development of a pH indicator composed of high moisture-absorbing materials for real-time monitoring of chicken breast freshness. *Food science and biotechnology*, 26(1):37-42.
- Kuswandi B, Nurfawaidi A. 2017. On-package dual sensors label based on pH indicators for real-time monitoring of beef freshness. *Food Control*, 82:91-100.
- Li C, Ma H, Venkateswaran S, *et al.* 2020. Highly efficient and sustainable carboxylated cellulose filters for removal of cationic dyes/heavy metals ions. *Chemical Engineering Journal*, 389:123458.

- Li D, Henschen J, Ek M. 2017. Esterification and hydrolysis of cellulose using oxalic acid dihydrate in a solvent-free reaction suitable for preparation of surface-functionalised cellulose nanocrystals with high yield. *Green Chemistry*, 19(23):5564-5567.
- Lin X, Li N, Xiao Q, *et al.* 2022. Polyvinyl alcohol/starch-based film incorporated with grape skin anthocyanins and metal-organic framework crystals for colorimetric monitoring of pork freshness. *Food Chemistry*, 395:133613.
- Liu J, Wang H, Guo M, Li, *et al.* 2019. Extract from *Lycium ruthenicum* Murr. Incorporating κ -carrageenan colorimetric film with a wide pH-sensing range for food freshness monitoring. *Food Hydrocolloids*, 94:1-10.
- Liu R, Chi W, Jin H, *et al.* 2022. Fabricating κ -carrageenan/carboxymethyl cellulose films encapsulating bromothymol blue fixed rice straw fiber for monitoring meat freshness. *Industrial Crops and Products*, 187:115420.
- Meng Q, Wang T J. 2019. Mechanics of Strong and Tough Cellulose Nanopaper. *Applied Mechanics Reviews*, 71(4).
- Milisav I, Ribaric S, Poljsak B. 2018. Antioxidant Vitamins and Ageing. *Sub-cellular biochemistry*, 90:1-23.
- Moon R J, Martini A, Naim J, *et al.* 2011. Cellulose nanomaterials review: structure, properties and nanocomposites. *Chemical Society reviews*, 40(7):3941-3994.
- Pacquit A, Lau K T, McLaughlin H, *et al.* 2006. Development of a volatile amine sensor for the monitoring of fish spoilage. *Talanta*, 69(2):515-520.
- Palmieri F, Estoppey A, House G L, *et al.* 2019. Oxalic acid, a molecule at the crossroads of bacterial-fungal interactions. *Advances in applied microbiology*, 106:49-77.
- Rahman S, Chowdhury D. 2022. Guar gum-sodium alginate nanocomposite film as a smart fluorescence-based humidity sensor: A smart packaging material. *International journal of biological macromolecules*, 216:571-582.
- Ran R, Wang L, Su Y, *et al.* 2021. Preparation of pH-indicator films based on soy protein isolate/bromothymol blue and methyl red for monitoring fresh-cut apple freshness. *Journal of food science*, 86(10):4594-4610.
- Rohaizu R, Wanrosli W D. 2017. Sono-assisted TEMPO oxidation of oil palm lignocellulosic biomass for isolation of nanocrystalline cellulose. *Ultrason Sonochem*, 34:631-639.
- Rong L, Zhang T, Ma Y, *et al.* 2023. An intelligent label using sodium carboxymethyl cellulose and carrageenan for monitoring the freshness of fresh-cut papaya. *Food Control*, 145:109420.
- Shi X, Wu P. 2021. A Smart Patch with On-Demand Detachable Adhesion for Bioelectronics. *Small*, 17(26):2101220.
- Spiewak R, Vankayalapati G S, Considine J M, *et al.* 2022. Humidity dependence of fracture toughness of cellulose fibrous networks. *Engineering fracture mechanics*, 264(1).
- Sun Y, Zhang M, Bhandari B, *et al.* 2019. Intelligent detection of flavor changes in ginger during microwave vacuum drying based on LF-NMR. *Food Research International*, 119:417-425.
- Teixeira S C, de Oliveira T V, Assis Silva R R, *et al.* 2022. Colorimetric indicators of açai anthocyanin extract in the biodegradable polymer matrix to indicate fresh shrimp. *Food Bioscience*, 48:101808.
- Wang A, Zhu Q, Xing Z. 2020. Multifunctional quaternized chitosan@surface plasmon resonance Ag/N-TiO₂ core-shell microsphere for synergistic adsorption-photothermal catalysis degradation of low-temperature wastewater and bacteriostasis under visible light. *Chemical Engineering Journal*, 393:124781.
- Wang H, Xie H, Du H, *et al.* 2020. Highly Efficient Preparation of Functional and Thermostable Cellulose Nanocrystals via H₂SO₄ Intensified Acetic Acid Hydrolysis. *Carbohydrate polymers*, 239:116233.
- Yang J, Fan Y, Cui J, *et al.* 2021. Colorimetric films based on pectin/sodium alginate/xanthan gum incorporated with raspberry

pomace extract for monitoring protein-rich food freshness. *International journal of biological macromolecules*, 185:959-965.

Yu F, Shi H, Wang K, *et al.* 2022. Preparation of robust and fully bio-based modified paper via mussel-inspired layer-by-layer assembly of chitosan and carboxymethyl cellulose for food packaging. *International journal of biological macromolecules*, 222(Pt A):1238-1249.

Zhang D, Yu S, Wang X, *et al.* 2022. UV illumination-enhanced ultrasensitive ammonia gas sensor based on (001)TiO₂/MXene heterostructure for food spoilage detection. *Journal of hazardous materials*, 423(Pt B):127160.